56th ANNUAL MIDWEST STUDENT BIOMEDICAL RESEARCH FORUM

Saturday, March 8, 2025

ROOM 3048

8:00 a.m.	O-83	IMMUNIZATION OF ARTHRITIS PRONE MICE WITH MALONDIALDEHYDE-ACETADLDEHYDE (MAA) MODIFIED VIMENTIN INDUCES FIBROTIC LUNG CHANGES Presenter: Wenxian Zhou
8:15 a.m.	O-60	OREXIN A AND B DYSREGULATION AFTER TRIPLE HYPOXIA-HYPERCAPNIA CHALLENGE IN PRECLINICAL MODEL OF SUDEP Presenter: Parisa Rafiei
8:30 a.m.	O-55	ALCOHOL USE IMPAIRS INNATE IMMUNE CELL METABOLISM AND EFFECTOR FUNCTION MOLECULE TRAFFICKING Presenter: Ashley Peer
8:45 a.m.	O-53	SYSTEMIC LUPUS ERYTHEMATOSUS AFFECTS OVARIAN DYSFUNCTION IN MICE Presenter: Ashley Pak
9:00 a.m.	O-43	MICROGLIA MORPHOLOGY AND PHAGOCYTIC ACTIVATION IN VISUAL BRAIN REGIONS OF THE 5XFAD MOUSE Presenter: Shaylah McCool
9:15 a.m.	O-41	ZINC-DEFICIENCY UPREGULATES BACTERIAL METALLOPHORE PRODUCTION AND EXACERBATES INTESTINAL EPITHELIAL BARRIER DISRUPTION IN A MOUSE MODEL OF INFLAMMATORY BOWEL DISEASE Presenter: Mason Mandolfo
9:30 a.m.	O-25	RE-EXPRESSION OF CX45 IN DISEASED MYOCARDIUM: IMPLICATIONS FOR ELECTRICAL COUPLING AND THERAPEUTIC TARGETING IN ARRHYTHMOGENESIS Presenter: Paras Gupta
9:45 a.m.	O-06	INVESTIGATING THE ROLE OF ASTROCYTES IN DEFICIENT SLEEP IN FRAGILE X SYNDROME MOUSE MODEL Presenter: Alexandria Anding
10:00 a.m.		**BREAK**

IMMUNIZATION OF ARTHRITIS PRONE MICE WITH MALONDIALDEHYDE-ACETADLDEHYDE (MAA) MODIFIED VIMENTIN INDUCES FIBROTIC LUNG CHANGES

Wenxian Zhou, Michael J. Duryee, Nozima Aripova, Jill A. Poole, Carlos D. Hunter, Amy J. Nelson, Bryant R. England, Ted R. Mikuls and Geoffrey M. Thiele (UNMC Omaha, NE)

Background, Significance, Hypothesis: Rheumatoid arthritis associated interstitial lung disease (RA-ILD) is the most overrepresented cause of death among RA patients, yet the mechanisms underlying lung fibrosis remain elusive. Recent studies have highlighted the role of malondialdehyde-acetaldehyde (MAA)-modified proteins in the pathogenesis of RA-ILD. This modification acts as a potent hapten, triggering autoimmune responses that are predictive of RA-ILD. Moreover, MAA-adducted proteins are enriched in lung tissues of RA patients and together with citrulline (CIT) induce macrophage-fibroblast cross talk leading to increased extracellular matrix deposition. The aim of this study was to examine whether immunization of mice with MAA-modified protein induces lung fibrosis.

Experimental Design: Arthritis prone male DBA/1J mice (n=5/group) were given weekly intraperitoneal injections for 5 weeks consisting of: 1) 25µg/mL of unmodified vimentin (VIM), 2) 25µg/mL of VIM-MAA, or 3) equal volumes of saline (additional negative control). Mice were sacrificed the sixth week. Lung tissues were resected, paraffin embedded, sectioned, and stained with trichrome (for total collagen deposition) or immunohistochemistry (IHC) using anti-MAA, anti-CIT, and anti-VIM antibodies. Dissociated lung tissues underwent analysis by flow cytometry to characterize immune cell infiltration. Mice were assessed for arthritis development using a semi-quantitative score that incorporates paw swelling and redness. Statistical analysis was performed using one-way ANOVA with Tukey's multiple comparisons test.

Results: Trichrome staining of lungs revealed increased collagen deposition in VIM-MAA immunized mice (vs. VIM or saline, $p<0.0001$) that was most prominent around sites of cellular infiltrate (Fig.1). Likewise, IHC staining demonstrated the highest expression of CIT ($p<0.05$), MAA ($p<0.01$), and VIM ($p<0.001$) antigens in the lungs of VIM-MAA immunized mice (Fig.2). MAA-modified proteins were co-localized with both CIT ($r^2 = 0.46$) and VIM ($r^2 = 0.33$). Flow cytometry of lung tissue revealed a significant increase in alveolar macrophages with VIM-MAA immunization vs. other groups (Fig. 3, $p<0.05$) but no other changes in myeloid cell subpopulations. In contrast, there was a decrease in CD4/CD8 T cells in mice immunized with VIM or VIM-MAA compared to saline controls ($p<0.0001$). There were no differences in arthritis scores across groups.

Conclusions: This study is the first to demonstrate that systemic immunity to MAA-modified vimentin directly contributes to lung fibrosis. In addition to demonstrating increased collagen and vimentin deposition, affected tissues were characterized by increased alveolar macrophages and expression of both MAA- and CIT-modified proteins accompanied by decreased T cell populations. An improved understanding of mechanisms linking VIM-MAA immunization with lung fibrosis using this model may provide much needed insight into the pathogenesis of RA-ILD.

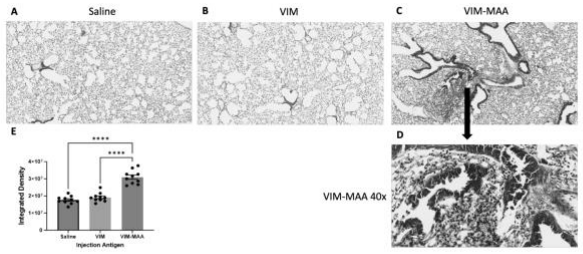

Figure 1. Trichrome staining of lung tissue in DBA/1J mice immunized with native and modified vimentin. Mice were immunized with saline, native VIM, and VIM-MAA. Panels A-D illustrate collagen deposition (blue color) on trichrome staining. Panel E demonstrates quantification of collagen deposition. Only significant differences between groups are illustrated: ****p<0.0001.

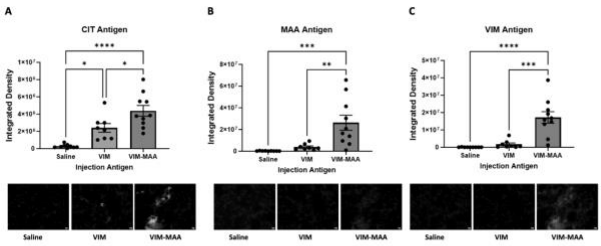

Figure 2. IHC staining of lung tissue in DBA/1J mice immunized with native and modified vimentin. CIT (Panel A), MAA (Panel B), and VIM (Panel C) antigen levels in lung tissues from mice immunized with saline, native VIM, and VIM-MAA. Representative lung tissue with IHC staining for antigens are shown below the quantified results. Only significant differences between groups are illustrated: ****p<0.0001, ***p<0.001, **p<0.01, *p<0.05.

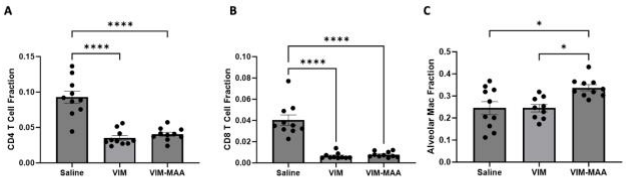

Figure 3. Flow cytometry of lung cells in DBA/1J mice immunized with native and modified vimentin. CD4+ T cell (Panel A), CD8+ T cell (Panel B), and alveolar macrophages (Panel C) in lung homogenates from mice immunized with saline, native VIM, and VIM-MAA. Only significant differences between groups are illustrated: ****p<0.0001, *p<0.05.

OREXIN A AND B DYSREGULATION AFTER TRIPLE HYPOXIA-HYPERCAPNIA CHALLENGE IN PRECLINICAL MODEL OF SUDEP

Parisa Rafiei, Shruthi Iyer, Timothy A. Simeone, Kristina A. Simeone

Department of Pharmacology and Neuroscience, Creighton University School of Medicine
Omaha, Nebraska

Background: Sudden Unexpected Death in Epilepsy (SUDEP) is one of the leading causes of death in people diagnosed with epilepsy. According to the MORTEMUS study, a generalized clonic seizure (GCS), repeated transient apnea and prolonged terminal apnea precede SUDEP. Approximately half of GCSs, 30% of partial seizures, and post-convulsive central apnea associate with hypoxia and hypercapnia. These blood gas changes are detected by central and peripheral chemosensors. Orexin A and B neurons reside in the lateral hypothalamus and are one of the central chemosensors that may be dysregulated. These neurons project to the respiratory nuclei including Locus Coeruleus (LC) and Nucleus Tractus Solitarius (NTS) for adaptive respiration. We have previously reported that *Kcna1*-null mouse model exhibit spontaneous recurrent seizures (SRS), intermittent apnea, and chronic intermittent hypoxia and SUDEP.
Significance of Problem: Previous study conducted in our lab has shown impaired chemoresponse to HH in SUDEP. It is unclear which respiratory nuclei in the brainstem are involved in this specific pathway which leads to adaptive respiration failure and SUDEP. Researching the activation of orexin neurons in response to repeated HH and the involvement of certain respiratory nuclei in adaptive respiration is significant to gain a better understanding of this respiratory event.
Hypothesis: The *Kcna1*-null mouse model of SUDEP have increased orexin neuron activation in response to repeated hypoxia-hypercapnia challenge.
Experimental Design: We used a novel test in which mice are exposed to an acute repeated hypercapnic-hypoxic (HH) challenge, to mimic the blood gas changes which occur prior to clinical SUDEP (Figure 1). Equal numbers of WT and SRS mice were divided to control and experimental triple HH cohorts. Following exposure to the triple HH challenge or normoxia for the same duration (controls), brains were post-fixed by transcardial perfusion and sectioned coronally. Using systemic random sampling and immunohistochemistry, sections were double-labeled for either Orexin A and Fos (a marker of neuronal activation), or Orexin B and Fos. We used fluorescence microscopy to acquire and analyze images. Statistics were conducted with GraphPad Prism 10.

Fig. 1: Severe Triple HH challenge. Challenges were administered for 3 minutes with brief normoxia intervals. CH: Challenge; H-H: Hypercapnia-Hypoxia.

Results: Triple HH exposure increased Orexin A activation (Orexin A^+) in WT controls ($p < 0.01$), whereas Orexin B^+ neurons were nonresponsive to triple HH ($p = 0.07$). In contrast, the activation of Orexin A neurons in response to triple HH was dysregulated in SRS mice when compared to controls ($P < 0.01$). Similar to the WT group, Orexin B^+ neurons were not sensitive to triple HH. Although not significant, the number of Fos^+ cells in the triple HH group was increased ($p = 0.9406$). The ongoing data collection and analysis will be finalized by late December 2024-early January 2025.
Conclusions: Our novel data highlights the complex role of Orexin A signaling in triple HH chemoresponse in controls, the divergent responses between Orexin A and B neurons to triple HH. In addition, data indicate a dysregulation of Orexin A response to triple HH in preclinical SUDEP.

ALCOHOL USE IMPAIRS INNATE IMMUNE CELL METABOLISM AND EFFECTOR FUNCTION MOLECULE TRAFFICKING

A.M. Peer[1], D.N. Villageliu[1], K.C. Cunningham[1], T.A. Wyatt[1,2,3,4], and D.R., Samuelson[1,5]

Departments of [1]Internal Medicine-Pulmonary Division; [2]Environmental, Agricultural and Occupational Health, University of Nebraska Medical Center, Omaha, NE, USA; [3]Alcohol Center of Research-Nebraska; [4]Department of Veterans Affairs Nebraska, Western Iowa Health Care System, Omaha, NE, USA; [5]Nebraska Food for Health Center, University of Nebraska-Lincoln, Lincoln, NE, USA.

Introduction: Alcohol misuse annually accounts for approximately 5% of all deaths. Alcohol misuse is a well-established independent risk factor for bacterial pneumonia. Our lab was the first to determine that gut dysbiosis due to alcohol misuse increases bacterial pneumonia risk. Previously, we demonstrated attenuated immune cell recruitment (NK cells, macrophages) to the lungs during bacterial infection in alcohol-fed mice. Furthermore, supplementation with indole, a metabolite produced by gut bacteria, restored lung NK cell recruitment. However, the mechanism in which immune cell function or trafficking is altered by alcohol is still unknown. Our current hypothesis is that alcohol modulates immune cell metabolism, resulting in modification of the cell effector function, including lytic molecule packaging, trafficking, and release, as well as decreased bacterial phagocytic clearance.

Methods: Utilizing both *in vitro* and *in vivo* models we evaluated alcohol effects on immune cell effector function and metabolism. Briefly, 8 to 12-week-old female C57BL/6 mice were placed onto a 20% vol/vol ethanol-containing water for 8 weeks. Control mice received water only. Mouse splenic NK cells were then isolated via a negative-selection based magnetic bead kit and cultured at 37°C in 5% CO_2 for 6 days in MyeloCult™ H5100 media containing 5% horse serum, 0.1 mM nonessential amino acids, 1 mM sodium pyruvate, 100 IU/ml penicillin, 100 ml/ml streptomycin, 0.05 mM 2-mercaptoethanol, and 1000 IU/ml of mouse IL-2. NK cell metabolism was then assessed using the XFp8 extracellular flux analyzer. The interplay between metabolism and immune cell effector lytic molecule packaging and trafficking to the immunological synapse before release was examined via fluorescence microscopy, ELISA, and Western blot. Finally, bone marrow-derived macrophages were generated from the femurs and tibias of each mouse and cultured in DMEM media containing 1 g/L glucose, L-glutamine, and sodium pyruvate, 5% FBS, 100 IU/ml penicillin, 100 ml/ml streptomycin, and 50 ng/mL of GM-CSF for 7 days. Macrophage metabolism was then assessed using the XFp8 extracellular flux analyzer, and phagocytosis was assessed using pHrodo red bioparticles.

Results: We established that NK cell bactericidal activity was dependent on the production of α-defensin and was decreased in NK cells isolated from alcohol-fed mice. We also discovered that NK cell immunometabolism is modulated via alcohol administration, demonstrated by an upregulation in glycolysis and a suppression of oxidative phosphorylation. Moreover, these metabolic changes were associated with diminished bacterial killing despite proficient effector molecule (e.g., granzyme, granulysin, perforin) production, with or without alcohol administration. Finally, we found that, like NK cells, macrophage immunometabolism is decreased via alcohol administration. Specifically, we found that macrophages treated from alcohol-fed mice exhibit upregulation in glycolysis and suppression of oxidative phosphorylation.

Conclusion: Together these data suggest that NK cell effector function and metabolism are significantly impaired by alcohol. These data also suggest that alcohol misuse increases bacterial pneumonia risk, in part, via metabolic disarrangement of NK cells and macrophages. However, the mechanism by which innate immune cell metabolism is impaired by alcohol and alcohol-related gut dysbiosis requires additional investigation.

SYSTEMIC LUPUS ERYTHEMATOSUS AFFECTS OVARIAN DYSFUNCTION IN MICE

[1]Ashley Pak, [2]Wonmi So, [2]LiGyeom Ha, [2]Rahul Kakalij, [2]Amirhossein Abazarikia, [2]Erika I. Boesen, [2]So-Youn Kim
[1]Creighton University School of Medicine; [2]University of Nebraska Medical Center; Omaha, NE

Background: Systemic Lupus Erythematosus (SLE) is a chronic autoimmune disease that damages multiple organs and is characterized by excessive pathogenic autoantibodies, hyperactivation of the immune system, and accumulation of immune complexes in target tissues. SLE predominantly affects women of childbearing age, making it one of the most gender-biased autoimmune diseases. Given its frequent diagnosis during reproductive years, increasing attention has been directed toward the impact of this chronic condition and its treatment on ovarian function. While it is known that common treatments for SLE, such as cyclophosphamide and corticosteroids, deleteriously affect ovarian function, pathogenic processes associated with SLE itself may also pose significant challenges to endocrine health and reproductive outcomes in affected patients.

Significance of Problem: The exact etiology of SLE and its effects on reproductive organs remain unclear. However, studies indicate that SLE accounts for nearly 10% of infertility cases globally. In a recent study involving 40 SLE patients, 45% experienced irregular menstruation, including menstrual disorders and amenorrhea, suggesting that SLE may influence fertility. More specifically, autoimmunity is known to affect the ovarian germ cells, leading to the decrease of primordial follicles—key components of the ovarian reserve that are critical for future endocrine function and fertility in women of reproductive age. Currently, emerging theories propose that the chronic inflammatory state associated with SLE damages ovarian function. Despite these insights, significant gaps remain in the current literature regarding the underlying mechanisms and causal factors driving ovarian damage in SLE, which contributes to the observed decline in ovarian function.

Hypothesis, Problem or Question: When mice develop autoantibodies similar to those observed in human SLE patients, they experience progressive kidney damage (lupus nephritis), culminating in early mortality at approximately 6–9 months of age. We hypothesize that the ovarian phenotype also undergoes significant changes as SLE disease activity worsens, ultimately resulting in ovarian dysfunction.

Experimental Design: To differentiate disease-specific causes of ovarian dysfunction from iatrogenic ones, this study utilized a well-established spontaneous model of lupus: the female (New Zealand Black × New Zealand White) F1 hybrid mouse (NZBWF1). These mice progressively develop autoantibodies, leading to lupus nephritis. Ovaries were collected from NZBWF1 mice at 34 weeks of age, corresponding to the median onset of albuminuria in this model. Ovarian histological characteristics were evaluated and compared among NZBWF1 mice with varying severity of SLE, 8-week-old NZBWF1 mice in the pre-disease state, and 16-month-old C57BL/6 control female mice. The numbers of ovarian follicles and corpora lutea were compared across control mice, 8-week-old NZBWF1 mice, and NZBWF1 mice with differing SLE severity.

Results/Data: Histological analysis revealed significant differences between SLE and control ovaries. In SLE ovaries, the surface epithelial cells were markedly disrupted, forming a disorganized multilayer of epithelial cells, whereas control ovaries maintained a single, organized epithelial cell layer. Additionally, the number of ovarian follicles was significantly reduced in SLE ovaries compared to controls. The remaining follicles, ranging from primordial to antral stages, were predominantly localized in the cortical region, with no follicles observed in the medullary area. The medullary region of SLE ovaries contained disorganized stromal cells, unidentified cellular aggregates, and prominent vascular structures. Most surviving follicles of all classes in mice with severe SLE exhibited abnormal morphology, including dying granulosa cells and disorganized theca layers. Notably, none of the SLE ovaries contained corpora lutea in any examined sections, whereas the ovaries of control mice and 8-week-old NZBWF1 mice consistently exhibited multiple corpora lutea.

Conclusions: The findings of this study support the hypothesis that significant histological changes occur in SLE ovarian tissue compared to ovarian tissues from 8-week-old NZBWF1 mice in the pre-disease state and 16-month-old normal control female mice. These changes include marked architectural disruptions, such as disorganized surface epithelial cells, reduced follicle numbers, and the absence of corpora lutea, all of which contribute to ovarian dysfunction. These results suggest that SLE-induced alterations may play a distinct role in the infertility observed in patients with SLE, separate from iatrogenic causes. Further research into the mechanisms underlying these changes will be critical for understanding the pathogenesis of SLE-associated ovarian dysfunction and its impact on ovarian reserves.

MICROGLIA MORPHOLOGY AND PHAGOCYTIC ACTIVATION IN VISUAL BRAIN REGIONS OF THE 5XFAD MOUSE

Shaylah McCool, Jennie C. Smith, Matthew Van Hook (UNMC, Omaha, NE)

Background: Vision changes are some of the first reported symptoms in Alzheimer's disease (AD), a neurodegenerative disorder characterized in part by the formation of extracellular amyloid beta (Aβ) plaques that lead to cognitive deficits, brain atrophy, and decreased quality of life for affected individuals. To better understand the changes occurring in the AD visual system, we aim to study how the immune system responds to the formation of pathological protein deposition in visual regions of the brain by examining microglia morphology and function. The dorsal lateral geniculate nucleus (dLGN) is a thalamic relay that receives input from the retina and sends it to the primary visual cortex (V1). Two other retinorecipient brain regions include the superior colliculus (SC), which is important for sensory-motor integration such as initiating and guiding eye movements, and the suprachiasmatic nucleus (SCN), which regulates circadian rhythms. We studied amyloid pathology and microglial responses in these four visual brain regions. To do this, we used the 5xFAD mouse model which develops Aβ plaques throughout the brain starting around 2 months of age.

Significance: In AD, microglia are no longer able to keep us with the Aβ plaque load found in AD patients leading to cognitive decline. Due to both the increasing number of individuals diagnosed with AD and its early impacts on vision in these patients, we aimed to provide an in-depth analysis of microglia in several visual regions of the brain as these cells are responsible for maintaining homeostasis and responding to disease pathology.

Hypothesis, Problem, or Question: How do microglia, the innate immune cells of the brain, respond to formation of Aβ plaques in visual brain regions?

Experimental Design: We used male and female 5xFAD mice at three timepoints – 6, 9, and 12 months of age. We performed immunohistochemistry on 50-µm-thick tissue sections containing a region of interest – dLGN, SC, SCN, or V1. We stained for Aβ plaques in each region using thioflavin s, and using fluorescence imaging techniques, we calculated the plaque density in each region. We co-stained for Iba1, a marker of microglia, and CD68, a lysosomal marker, which allowed us to correlate microglia morphology with its function. A 2-photon microscope was used to capture images of the dLGN, SCN, SC, and V1. A skeleton analysis was performed on 6, 9, and 12mo dLGN as well as on 9mo dLGN, SCN, SC, and V1 to quantitatively examine microglia morphology. We also calculated the percent of CD68 colocalized with Iba1 to determine changes in microglial phagocytic activity. Co-staining for Iba1 and thioflavin s was used to examine whether the microglia colocalize with plaques in these regions.

Data/Results: We found a relatively high density of Aβ plaques in the dLGN of the 5xFAD mice; yet did not find plaques in the SC or SCN. Looking at the primary visual cortex, we found a significant number of plaques in the 5xFAD mice compared to controls, but a significantly lower density than in the dLGN. There was also significantly increased plaque density at 60-80% depth in V1. The skeleton analysis showed decreased branch length and fewer endpoints per microglia in the dLGN at all timepoints indicative of microglia reactivity. We also found slightly decreased microglia branch length in the 9mo SCN. We did not see changes in branch length or endpoints per microglia in the SC or in V1. The Iba1/CD68 co-stain revealed a significant colocalization of CD68 with microglia the 6, 9, and 12mo 5xFAD dLGN with no change in any of the other three regions.

Conclusions: We found Aβ plaques throughout the brain in the 5xFAD model including visual regions such as the dLGN and V1. However, other key retinorecipient brain regions like the SC and SCN were devoid of plaques even up to 9mo of age. In regions with plaques, we found a significant change in microglia morphology toward an amoeboid state as well as significant colocalization with CD68 indicating phagocytic activity in plaque-infested areas. These results suggest amyloid pathology drives microglia activation and phagocytic activity in only a subset of visual areas of the 5xFAD brain.

ZINC-DEFICIENCY UPREGULATES BACTERIAL METALLOPHORE PRODUCTION AND EXACERBATES INTESTINAL EPITHELIAL BARRIER DISRUPTION IN A MOUSE MODEL OF INFLAMMATORY BOWEL DISEASE

Mason S. Mandolfo, Christi M. Ellis, Kelly C. Cunningham, Deandra R. Smith, Daren L. Knoell, Derrick R. Samuelson

University of Nebraska Medical Center, Omaha, NE

Background: Elevated levels of Lipocalin-2 and Calprotectin in feces are strongly associated with Inflammatory Bowel Disease (IBD). Both trace metal binding proteins are thought to reduce inflammation by preventing bacteria from acquiring essential trace metals, such as zinc (Zn) and iron (Fe). In addition, Zn and Fe deficiencies are common in patients diagnosed with IBD. These factors suggest the gut microbiome of patients with IBD may lack necessary levels of these trace metals. Trace metal starvation is known to cause bacteria to upregulate the production of metal-scavenging molecules called metallophores. We hypothesize that increased production of metallophores by the gut microbiome could contribute to intestinal epithelial barrier disruption and exacerbate symptoms of IBD (Figure 1).

Methods: C57BL/6 mice were fed a Zn-deficient diet or a control diet for 3-weeks to establish a Zn deficiency. Fecal samples were then collected from individual mice following a 5-day treatment with 2.5% dextran sodium sulfate (DSS) or water control. mRNA was extracted, and qPCR targeting genes required to produce bacterial metallophores was performed. For *in vitro* experiments, enterobactin (Ent), a major bacterial metallophore, was prebound to either Zn, Fe, or nothing (apo-form) before use. Cytokine production was quantified using ELISAs. Intestinal organoids were derived from WT C57BL/6 mice. ZO-1 and Claudin-2 organization were assessed via immunofluorescent confocal imaging.

Results: We found that mRNA expression of metallophore-producing genes in the feces of DSS-treated mice was significantly increased compared to the vehicle control group. Some, but not all, target genes displayed an additive effect when mice were also on a Zn-deficient diet. We then evaluated the effects of Ent using *in* vitro cell culture models. We showed that treatment with apo-Ent induced cell death in C2BBe1 cells. We also showed induction of inflammatory cytokine production, such as IL-8 and INF-y. Interestingly, when treated with Fe-bound Ent, these effects were mitigated. Conversely, when treating with Zn-bound Ent, we saw an exacerbation of both cell death and inflammatory cytokine production. Finally, in a intestinal organoid model, we found that Ent treatment led to a significant disruption of tight junctional protein organization (Figure 2).

Conclusion: These results demonstrate increased metallophore production by the gut microbiota in mouse model of IBD. These data further show that metallophore production and disease severity are exacerbated by Zn deficiency. Similarly, we found that Ent disrupts intestinal epithelial barrier function by inducing cell death, inflammatory cytokine release, and tight junction protein dysregulation. Future studies will seek to quantify Ent in fecal samples and to link metallophore-producing bacteria to Zn deficiency in human participants.

RE-EXPRESSION OF CX45 IN DISEASED MYOCARDIUM: IMPLICATIONS FOR ELECTRICAL COUPLING AND THERAPEUTIC TARGETING IN ARRHYTHMOGENESIS

Gupta Paras, Stephen Sobota, and Paul L. Sorgen. UNMC Omaha, NE

Background, Significance, and Hypothesis: Connexins, particularly Cx43 and Cx45, are essential for electrical coupling in the myocardium, coordinating ventricular contractions. In the adult heart, Cx43 is the dominant connexin in the ventricular myocardium, while Cx45 is largely absent, confined to surrounding tissues such as nodal, epithelial, and fibroblast cells. In ventricular pathologies, remodeling of Cx43 at the intercalated discs disrupts gap junction localization, significantly increasing the risk of arrhythmias. Following initial myocardial injury, advanced remodeling involves two key processes: hypertrophy of the surrounding cardiac tissue and the re-expression of Cx45 in the ventricular myocardium. Hypertrophy serves as a compensatory response to myocardial loss and increased stress on the heart. Simultaneously, Cx45 reappears at the intercalated discs, forming homomeric and heteromeric channels with Cx43 that phenotypically function as Cx45 channels. In contrast to Cx43, Cx45 channels are characterized by lower conductance and higher voltage sensitivity, which would impair electrical impulse propagation in the ventricles. This aberrant signaling leads to uncoordinated atrial and ventricular contractions, driving arrhythmogenesis. Despite its evident role in cardiac pathology, the mechanisms underlying Cx45's re-emergence and its impact on disease progression remain poorly understood. We **hypothesize** that the temporal regulation of Cx45, in conjunction with Cx43, alters gap junction dynamics, electrical conduction, and drives arrhythmogenesis in advanced cardiac disease. Targeting connexin function represents a promising therapeutic strategy for restoring electrical stability and preventing arrhythmias in cardiac disorders.

Experimental Design: To investigate this hypothesis, we will utilize iPSC-derived cardiomyocytes (iPSC-CMs) cultured on micro-electrode arrays (MEAs) to assess electrical activity. We first will examine the effects of overexpressing Cx43, Cx45, or both on electrical conduction and action potential characteristics. This will be followed by Cx45 knockdown in Cx43/45-overexpressing cells to evaluate functional rescue mechanisms. To model hypertrophy, mimicking myocardial remodeling in advanced pathology, we will treat iPSC-CMs with pharmacological agents such as angiotensin and endothelin-1 and assessed their impact on connexin function and arrhythmogenesis. Furthermore, molecular techniques will be employed to investigate connexin trafficking, post-translational modifications, and degradation pathways.

Data and Results: Preliminary work has been done to generate the iPSC-CM model. Current work involves optimizing iPSC-CMs plating on the MEA, for electrical readings, and Cx43/Cx45 overexpression with the viral AAV6 vectors.

Conclusion: This study aims to model the molecular and functional role of Cx45 re-emergence in the diseased myocardium, focusing on its impact on electrical physiology and arrhythmogenesis. By using iPSC-CMs, MEA technology, and molecular tools, we aim to identify key mechanisms that govern cardiac electrical disfunction and explore therapeutic interventions to correct connexin dysregulation in advanced cardiac pathology. Ultimately, these findings contribute to the development of novel treatments for cardiac disorders linked to connexin dysfunction.

INVESTIGATING THE ROLE OF ASTROCYTES IN DEFICIENT SLEEP IN FRAGILE X SYNDROME MOUSE MODEL

A. Anding, P. Ragunathan, P. Zhong, A. Dunaevsky

University of Nebraska Medical Center (Omaha, Nebraska)

Background, Significance, Hypothesis: Fragile X syndrome (FXS) is the most common form of inherited intellectual disability, and the leading monogenic cause of autism spectrum disorder. Pediatric clinical polysomnography studies show that children with FXS suffer rapid-eye movement (REM) sleep deficiency, which is a grossly understudied phenotype in animal research. The consequences of sleep deprivation have negative effects on cognition, emotional processing, and several aspects of physical health and overall quality of life, but the mechanics of sleep deficiency in FXS are not fully understood.

While neurons are the most commonly targeted cell type in FXS studies, our lab has shown that astrocytes, a subtype of glial cell in the central nervous system, display an abnormal increase in cytosolic calcium (Ca^{2+}) events in a mouse model of FXS (Fmr1 KO), a trait that contributes to behavioral symptoms. Recently, astrocytic Ca^{2+} activity has also been heavily implicated in sleep neurophysiology. However, whether altered cortical astrocyte Ca^{2+} events in FXS contributes to sleep impairments, has not been explored. *Our hypothesis is that sleep impairments in Fragile X syndrome are driven by aberrant calcium signaling in cortical astrocytes.*

Experimental Design: In this ongoing study, we perform simultaneous cortical electroencephalography (EEG), electromyography (EMG) recordings and behavioral monitoring in Fmr1 KO and astrocyte-deleted Fmr1 cKO mice using telemetry devices to examine electrophysiological architecture associated with sleep and wake cycles in FXS, and determine the role of astrocytes in mediating sleep impairments. Telemetry data is also recorded in mice after undergoing prolonged sleep deprivation to determine whether sleep homeostasis is disrupted. Finally, we are also performing in vivo multiphoton calcium imaging in Fmr1 KO mice to examine astrocyte signaling patterns during sleep and wake.

Results: Fmr1 KO mice show a NREM (non-rapid eye movement) sleep deficit across development, but no REM deficit. These mice also displayed impaired sleep homeostasis, indicated by lower NREM sleep following sleep deprivation compared to wild-type littermate mice. In determining whether astrocytic Fmr1 expression could be driving sleep deficits, astrocyte-deleted Fmr1 cKO mice did not display a sleep deficit in the light phase (mouse resting phase) or dark phase (mouse active phase). Preliminary results from in vivo imaging have revealed that astrocytic Ca^{2+} signals exhibit distinct features across the sleep/wake cycle, and hyperactive Ca^{2+} signaling may contribute to sleep impairment.

Conclusions: This is the first study to investigate whether altered cortical astrocyte Ca^{2+} activity contributes to FXS sleep deficiency. While Fmr1 KO mice display sleep impairments in early development and in adults, Fmr1 astrocyte cKO mice do not show sleep deficit, so our preliminary conclusion is that lack of astrocytic Fmr1 expression is not the primary driver of sleep impairments in FXS. However, this conclusion does not negate the potential effect hyperactive astrocyte Ca^{2+} may have on overall sleep physiology. Future imaging experiments will allow the direct observation of astrocyte Ca^{2+} dynamics during FXS sleep-wake cycles, providing critical insights into how these cellular activities may influence sleep architecture and contribute to the broader understanding of FXS-related sleep disturbances.